J MATER SCI **41** (2006) 2703–2710

The melting behavior of faceted particles embedded in the solid state: A family of Wulff shapes

E. J. SIEM*
Centre de Recherche en Matière Condensée et Nansciences–CNRS, Campus de Luminy, Case 913, 13288, Marseille Cedex 9, France
E-mail: esiem@crmcn.univ-mrs.fr

E. JOHNSON
Nano Science Center, Niels Bohr Institute, University of Copenhagen, Universitetsparken 5, DK-2100, Copenhagen Ø, Denmark; Department of Materials Research, Risø National Laboratory, DK-4000, Roskilde, Denmark

Published online: 17 April 2006

We consider the melting behavior of nanoscale particles embedded in a crystalline solid. Calculations of three-dimensional shapes following from a minimization of interfacial free energy show that melt configurations depend on the melt volume fraction, particle shape, and the relative energy densities of particle interfaces. Five members of the family of Wulff shapes with cubic symmetry containing only {111} and {100} facets are studied in detail. Although general trends are noted, the melting behavior is found to be complex and strongly dependent on particle shape. We assume that the melt volume is located in one contiguous region. In such a case, the driving force to replace high-energy facets *decreases* with the relative energy of those facets.

1. Introduction

The melting behavior of particles embedded in the solid state has implications in many material properties—for instance, the mechanical integrity of a material at high temperatures. Because the behavior of small particles often deviates from that of their bulk analogues, the topic is one of academic, as well as practical, interest. Both the melting temperature and melting behavior of a solid particle depends on its size [1], its shape, and the anisotropy of its interfacial free energy density, $\gamma(\hat{n})$ [2].

In the simplest case, the shape of an equilibrated particle of fixed volume is directly related to its $\gamma(\hat{n})$. This shape—the Wulff shape, $\mathcal{W}$—is the shape that minimizes the interfacial free energy of the particle at constant temperature [3]. Embedded particles that have achieved their $\mathcal{W}$ are frequently observed through methods of transmission electron microscopy (TEM) [4]. Particles observed in cubic systems often display the following two characteristics: they are faceted, containing both {100} and {111} facets in proportions dependent on the ratio $\gamma_{100}/\gamma_{111}$; and they maintain a cube-on-cube orientation relationship with the embedding grain, meaning that the crystal axes of the particle and grain are kept parallel. (Throughout, γ_{hkl} denotes the interfacial free energy density of the $\{hkl\}$ family of facets.)

Particles that melt at a temperature below the matrix can be studied through *in-situ* TEM. Of interest for this work, *in-situ* TEM has indicated that indium particles in dilute aluminum alloys melt in distinct stages when the particles are larger than a few nanometers and allowed to equilibrate after each temperature increment [5–7]. The stages are classified by which of the {111} and {100} solid particle/solid matrix facets are replaced with *melted* particle/solid matrix interface. Transitions between the stages occur when the particle melt grows and moves to new facets. To a first approximation, the position of the particle/matrix interface remains fixed during melting, and transitions between stages require the particle melt to make, in some cases, large geometric rearrangements.

Recent investigations combining *in-situ* TEM with a numerical analysis suggest that: (1) the stages observed in previous studies are approximately followed by

*Author to whom all correspondence should be addressed.
0022-2461
DOI: 10.1007/s10853-006-7873-0

TABLE I The Υ value and relationship between facet free energies for the five $\mathcal{W}$ of interest

Shape	$\Upsilon = \gamma_{100}/\gamma_{111}$	
Cube	$0.577 \approx \frac{1}{\sqrt{3}}$	$\sqrt{3}\gamma_{100} = \gamma_{111}$
Cuboctahedron	$0.866 \approx \frac{\sqrt{3}}{2}$	$\gamma_{100} = \frac{\sqrt{3}}{2}\gamma_{111}$
Truncated octahedron	1.000	$\gamma_{100} = \gamma_{111}$
Truncated octahedron	$1.155 \approx \frac{2}{\sqrt{3}}$	$\frac{\sqrt{3}}{2}\gamma_{100} = \gamma_{111}$
Octahedron	$1.732 \approx \sqrt{3}$	$\gamma_{100} = \sqrt{3}\gamma_{111}$

TABLE II Contact angles between melt and both {100} and {111} matrix facets for each shape. These angles follow from the fixed set of free energy ratios applied in the calculations

Υ	$\theta_{M/100}$ (°)	$\theta_{M/111}$ (°)
0.577	80.03	N/A
0.866	74.94	72.54
1.000	72.54	72.54
1.155	69.73	72.54
1.732	N/A	72.54

lead-indium particles embedded in dilute aluminum alloys, and (2) these stages are defined by configurations that minimize interfacial free energy for a fixed melt volume fraction, V_M [8]. This work extends the numerical analysis to consider the coupled effect of particle shape and interfacial free energy on the set of energy-minimizing melt configurations. For simplicity, the analysis is confined to the family of polyhedral shapes with cubic symmetry that contain only {100} and {111} facets and differ in the ratio $\Upsilon = \gamma_{100}/\gamma_{111}$. This family extends from a cube, which occurs for $\Upsilon \leq 0.577$, to an octahedron ($\Upsilon \geq 1.732$). Five members of the family, shown in Fig. 1, are presented here: a cube of $\Upsilon = 0.577$, the cuboctahedron ($\Upsilon = 0.866$), an energetically simple truncated octahedron ($\Upsilon = 1$), a truncated octahedron approximating the shape often observed for lead particles in dilute aluminum alloys ($\Upsilon = 1.155$) [9], and an octahedron ($\Upsilon = 1.732$). As shown in Table I, these values for Υ produce a systematic, informative study.

2. Computational methods

2.1. Assumptions

Five interfaces, labeled (a)–(e) in Fig. 2, were necessary for the calculations. Two, (a) and (b), are between solid particle and solid matrix facets; two, (c) and (d), are between *melted* particle and solid matrix facets; and one, (e), separates the solid and melted portions of the particle. The following relative interfacial free energies where fixed:

$$\gamma_{100} = \Upsilon\gamma_{111} \quad \gamma_{M/100} = \frac{9}{10}\gamma_{100}$$

$$\gamma_{M/111} = \frac{9}{10}\gamma_{111} \quad \gamma_M = \frac{1}{3}\gamma_{111}$$

where γ_{hkl} refers to the solid particle/solid matrix interfacial free energy density, $\gamma_{M/hkl}$ refers to that of the melted particle/solid matrix, and γ_M refers to that of the solid/melted particle. These values were selected to produce results that follow observed melting behavior (discussed below) while avoiding numerical instabilities that occur when the conditions for perfect wetting are met. As in [8], the solid/melted particle interface is called the *internal melt interface*.

Table II provides a physical interpretation of the relative energy densities, listing the contact angle between a drop of particle melt and a {100} matrix facet and that between a drop and a {111} facet for each Υ. Two observations can be made from a cursory glance at the table: (1) the contact angles are close to 90°, and (2) the particle melt/solid matrix interfacial free energy is taken to be anisotropic. Both assumptions follow from TEM observations of Pb and In particles in Al. For (1), contact angle measurements have shown that the melted particle/solid matrix interface has a free energy density that is not too different from the incoherent solid particle/solid matrix interface [7, 8]. For (2), weak anisotropy of melted Pb particle/solid Al

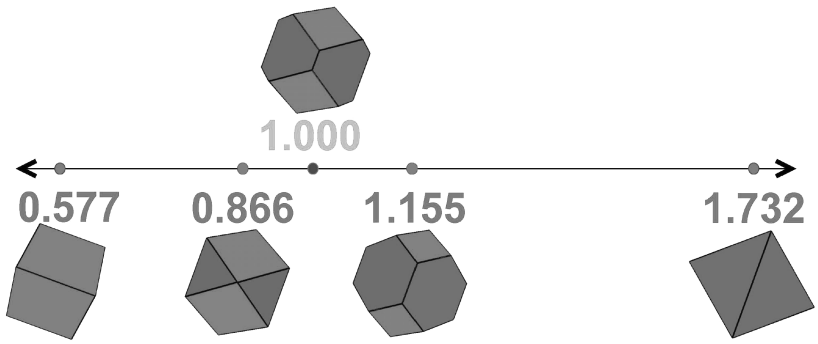

Figure 1 The five particle shapes used in this study are members of a family of shapes extending from a cube to an octahedron. The five shapes are: a cube ($\Upsilon = 0.577$), the cuboctahedron (0.866), two truncated octahedra (1 and 1.155), and an octahedron (1.732). As Υ increases, the {100} facet free energy becomes so large that the size of the {100} facets decreases and the distance between {100} facets increases.

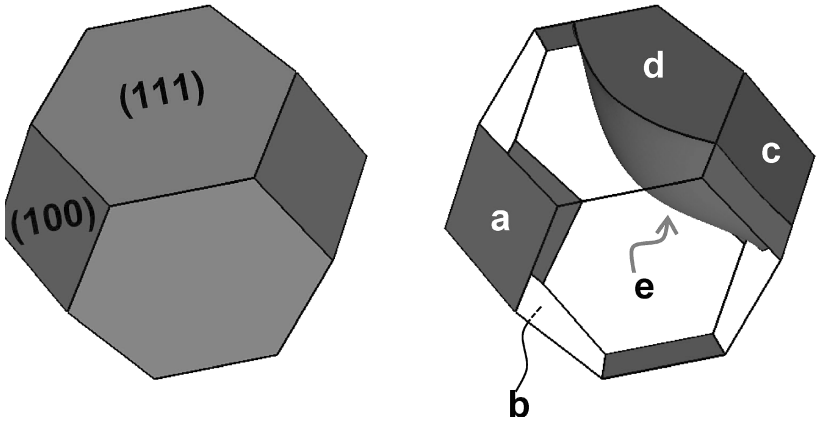

Figure 2 (*Left*) The truncated octahedra of $\Upsilon = 1.155$ is used as an example to indicate which facets are {111} (here perfect hexagons) and which are {100} (squares). (*Right*) The five interfaces: (a) solid particle/solid matrix {100}, (a) solid particle/solid matrix {111}, (c) melted particle/solid matrix {100}, (d) meltedparticle/solid matrix {111}, and (e) solid particle/melted particle.

matrix interface has been established [10]. The fourth of the above energy relationships was chosen to reflect the small value that an interface separating a solid from its melt generally takes [11].

The following additional assumptions have been made to better isolate the effect of particle shape on melt configuration. It is assumed that the particle volume (melt + solid) is convex and completely enclosed by {100} and {111} matrix facets, that the position of the particle/matrix interface is fixed, that the internal melt interface divides the particle into two contiguous regions, that the internal melt interfacial free energy is isotropic, and that the relative values of interfacial free energy do not change during melting.

The last assumption is not generally valid because the composition of the melt should change with gradual changes in temperature. However, this assumption is not too unreasonable, as it produces qualitative results that agree with observations of particles melting in dilute Al alloys [8].

2.2. Configurations

Details of the methods used to obtain the energy-minimizing melt configurations are given elsewhere [8]. Briefly, the particle $\mathcal{W}$ were calculated with *Wulffman* [12], and the equilibrium melt configurations were calculated as a function of the fraction of particle melted, V_M, with the *Surface Evolver* [13].

To determine the "equilibrium melt trajectory" for each Υ—i.e., the sequence of melt configurations that, on increasing V_M, give the minimum interfacial free energy with respect to all other configurations—several possible melt configurations were tested for each V_M. Thirteen configurations were tested for the cube, eighteen for the shapes bounded by both {100} and {111} matrix facets, and fourteen for the octahedron. Although more than eighteen configurations are possible for each shape, the tests were limited to those configurations for which interfacial free energy minima were suspected. Among those tested, less than half gave energy minima.

2.3. Stability

For a fixed V_M, not all configurations were found to be stable. Generally, changing V_M leads to either a *touching* instability, which occurs when the set of facets touched by the melt changes, or a *necking* instability, which occurs when the melt or solid divides so as to produce multiple internal melt interfaces. When a configuration is stable, it is metastable with respect to configurations giving a lower total interfacial free energy, and it forms a portion of the equilibrium melt trajectory when there are no lower-energy configurations.

3. Results and discussion

The results differ slightly from those reported previously [8] because, here, a different set of interfacial free energies has been applied, and melted particle/solid matrix anisotropy has been introduced. The equilibrium melt trajectory configurations for the cube are shown in Fig. 3, and those for the cuboctahedron in Fig. 4. The truncated octahedra share the same basic trajectory (Fig. 5) with transitions between configurations for $\Upsilon = 1.000$ occurring at different V_M than those for $\Upsilon = 1.155$. Results for the octahedron are shown in Fig. 6.

To compare the total interfacial free energy necessary for a configuration, E, between shapes at a fixed V_M, a quantity that is independent of the particle's size, $E/V^{2/3}$, was used. The results are presented by first discussing general trends and then reviewing the five particle shapes individually.

3.1. General trends

The first trend to note, illustrated with the unmelted and completely melted particles in Table III, is that $E/V^{2/3}$

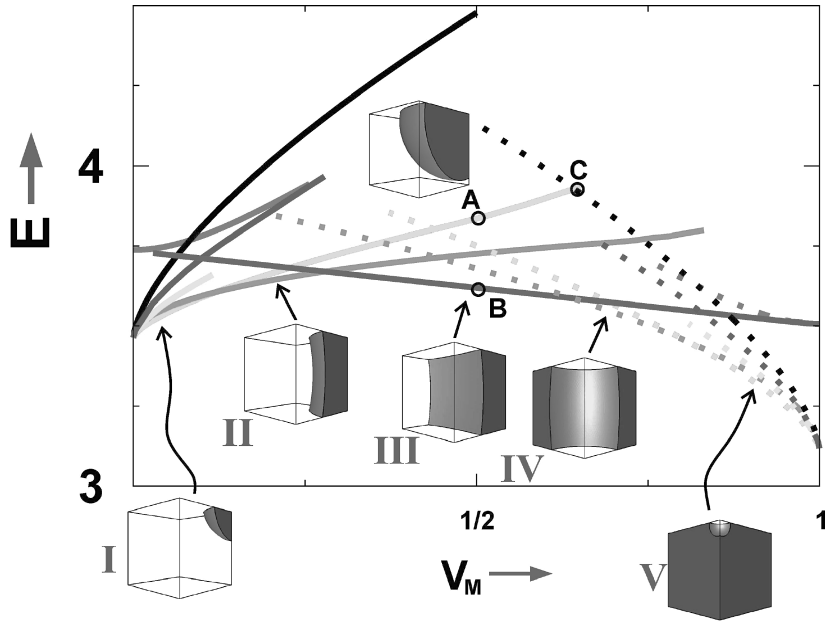

Figure 3 The melt trajectory of the cube consists of five configurations, shown below the plot of $E/V^{2/3}$ versus V_M that was obtained with the 13 configurations tested for the cube. The configuration stable at the lowest V_M becomes metastable with respect to other configurations at $V_M \sim 0.12$; the metastable state at $V_M = 0.5$ is indicated with point **A** and the stable state with **B**. A touching instability occurs at **C**.

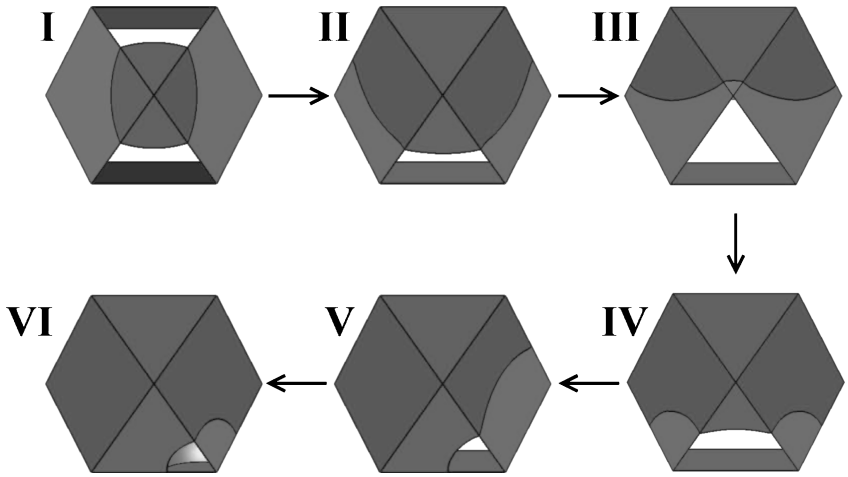

Figure 4 The melt trajectory of the cuboctahedron consists of six configurations.

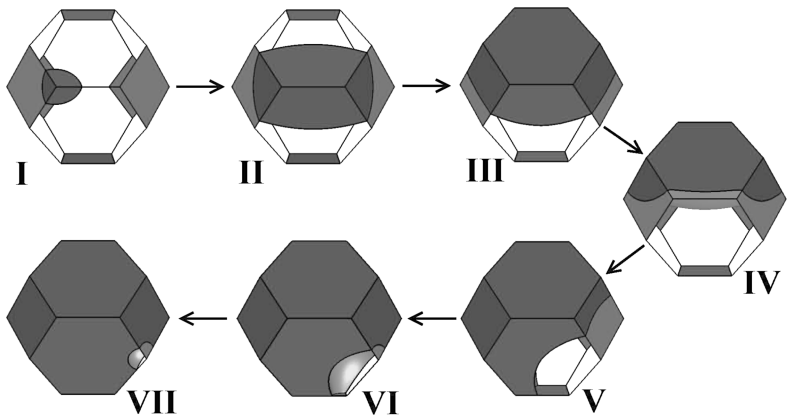

Figure 5 The melt trajectories of the two truncated octahedra share the same basic configurations, shown here for $\Upsilon = 1.155$.

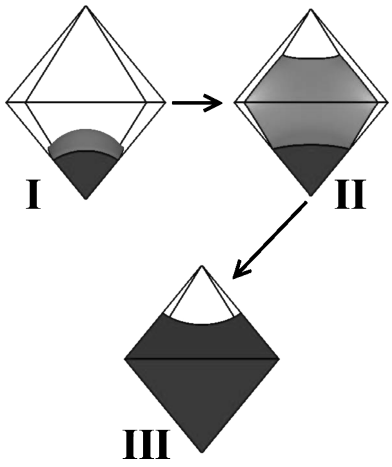

Figure 6 The melt trajectory of the octahedron consists of three configurations. Calculations suggest that a configuration for which the melt replaces two corners and portions of four {111} facets is in equilibrium with **I** and **II** at the transition between **I** and **II**.

increases as Υ increases. This result is due to the different values of interfacial free energy assigned to facets of different Υ . That is, $E/V^{2/3}$ is lower for shapes of smaller Υ because the total interfacial free energy of those shapes is proportional to Υ. The proportionality constant is dependent on shape, however, because Υ is the ratio of interfacial free energy densities and does not directly indicate the relative amounts of each type of interface—as Υ is increased from 0.577 to 1.732, the relative interfacial free energy of {100} interface increases but the amount of {100} interface decreases more quickly. If the interfacial free energy densities were independent of facet orientation, one would find that $E/V^{2/3}$ would be largest for the cube and lowest for a truncated octahedron with a slightly smaller area fraction of {100} facets than the shape constructed for $\Upsilon = 1.155$ (see [8] appendix).

The second trend is that, for a given Υ , there is a small maximum in E with changes to V_M before half of the particle has melted ($V_M < 1/2$). Interfacial energy increases at low V_M because melting increases the total amount of interface. Although the energy densities of the particle melt interfaces are relatively low, they are not low enough to compensate for this increase. Beyond the maximum,

TABLE III The total interfacial free energy divided by the squared cube root of the total (melt + solid) volume of the particle for each shape at $V_M = 0$ and $V_M = 1$. The quantity increases with Υ because it is dependent on Υ

Υ	$E/V^{2/3}$ (Solid particle)	$E/V^{2/3}$ (melted particle)
0.577	3.46	3.12
0.866	4.89	4.40
1.000	5.25	4.72
1.155	5.50	4.95
1.732	5.72	5.15

which occurs at the transition between configurations **I** and **II** in Fig. 7, energy is eliminated because the melt replaces increasingly more solid particle/solid matrix interface for smaller (or negative) increments to the internal melt interface.

As the last trends noted, the plot of E versus V_M generally has negative concavity ($d^2E/dV_M^2 < 0$) because the decrease in energy due to the replacement of solid particle/solid matrix interfaces becomes more significant than the increase in energy due to the creation of internal melt interface as the melt grows. However, a plot of E versus V_M has positive concavity ($d^2E/dV_M^2 > 0$) when changing V_M changes the internal melt interface but does not affect the amount of solid particle/solid matrix interface replaced.[1] Positive concavity indicates that it becomes increasingly difficult to change melt volume fraction from the V_M giving the minimum in energy. Such a case occurs when the melt interface is "pinned" at edges and corners of the particle shape. For instance, when the melt is attached to and completely replaces a {100} interface, additions to the melt volume could cause the melt to grow toward the particle center rather than migrate to neighboring facets. TEM observations of a PbIn particle in Al show that such "pinning" is not unusual, and an example is shown in Fig. 7, where the melt is pinned at the corners of two adjacent {100} facets. The calculation in this example uses $\Upsilon = 1.245$, the value obtained from a micrograph of the solid particle.

3.2. Case 1: The cube, $\Upsilon = 0.577$

The sequence of configurations comprising the melt trajectory of the cube for $\Upsilon = 0.577$ was obtained from the plot of $E/V^{2/3}$ versus V_M in Fig. 3. As shown, each of the five configurations gives the lowest energy curve for a range of V_M. Where curves cross, there is no driving force to change from one to another of the configurations described by those curves because they are energetically equivalent. Each of the melt trajectory configurations becomes metastable when its energy becomes greater than that of another. An example is shown at point **A**, which appears at $V_M = 1/2$ on the metastable extension of configuration **I**. A melt at **A** would reduce its energy by an amount proportional to the distance between **A** and **B** by adopting the energy-minimizing configuration at $V_M = 1/2$. Configuration **I** can persist in a metastable state with increments to V_M until reaching a touching instability at point **C**.

For the cube, the melt prefers a single corner for the lowest melt volume fractions ($V_M < 0.12$, **I**), two adjacent corners for $0.12 < V_M < 0.28$ (**II**), one face and portions of the four abutting faces for $0.28 < V_M < 0.64$

[1]There are exceptions. For instance, when the melt exists as a sphere with its origin at the particle's center of gravity, it produces an energy curve of negative concavity.

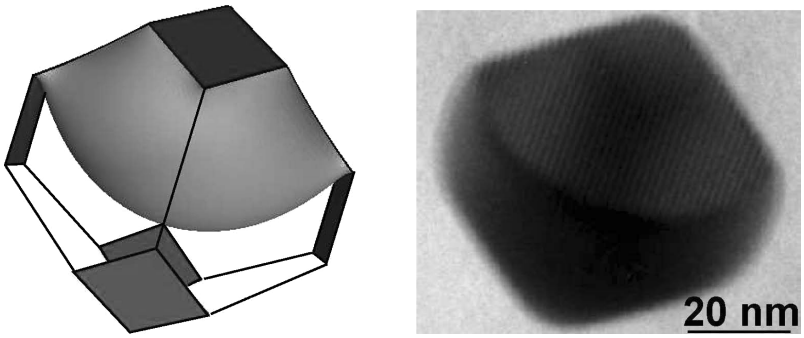

Figure 7 (*Left*) An example of a "pinned" internal melt interface that corresponds to the micrograph of a melting PbIn particle in Al (*right*). For this case, the calculated configuration was obtained for $\Upsilon = 1.245$, the aspect ratio measured from a TEM micrograph of a the solid PbIn particle.

(**III**), all but two adjacent corners for $0.28 < V_M < 0.81$ (**IV**), and all but one corner for $0.81 < V_M$ (**V**). Eight of the tested configurations do not form part of the melt trajectory.

Configurations **I** and **V**, and configurations **II** and **IV**, are closely related, differing only in which side of the internal melt interface that the melt is located and the details of the internal melt interface shape. Such configurations are called "inverses" of one another. Note that when one configuration meets an instability at $0 < V_M < 1$ (indicated in the plot by the termination of its energy curve), its inverse does not generally meet an instability at $1 - V_M$ because the contact angle between the internal melt interface and melted particle/solid matrix facets is not 90°. For instance, configuration **I** exists for a larger range of V_M than its inverse (**V**) because the contact angle is less than 90°. If the contact angle were larger than 90°, configuration **V** would have the larger range of stability.

In the limit of $V_M = 0$, there is but one configuration: the particle is completely solid. Here, a particle of unit volume will have an interfacial free energy of $6 \times 0.577 \approx 3.46$ (Table III). Similarly, for $V_M = 1$, the particle is completely melted, and a unit volume will have an energy of approximately 3.12. As shown in Fig. 1, not all configurations approach these limits smoothly. This result occurs because particular configurations, e.g., **III**, require that the melt replace a finite portion of solid particle/solid matrix interface.

Two additional features of the plot in Fig. 1 are discussed here. First, the energy curves describing configurations **I** and **II** change from negative to positive concavity on increasing V_M. These curves have inflection points because, as the melt grows, previously unpinned internal melt interface becomes pinned at corners in the particle shape, giving the positive concavity discussed in Section 3.1. The second feature is unique to the cube: there is a configuration for which energy is linearly related to changes in V_M. The energy of configuration **III** decreases linearly with increments in V_M because the internal melt interface maintains a constant shape, and additions to the melt simply push the position of this interface into the solid portion of the particle, replacing a fixed amount of solid particle/solid matrix interface with each addition.

The results shown in Fig. 1 apply to a two-phase system confined within a cubic cavity where the two phases are separated by an isotropic interface. The results are supported by those from a study for which the two phases are separated by an anisotropic interface that forms only {100}-type facets [14]. In that study, the degree of partial wetting between one phase and the walls of the cavity is varied in addition to the volume fraction of that phase. The study shows that, for the analogue of a contact angle of $\sim 80°$, the phase takes a cube shape and sits in one corner of the cube cavity for $V_M \lesssim 0.05$, replaces two adjacent corners and the edge connecting them (taking a rod shape) for $0.05 \lesssim V_M \lesssim 0.25$, replaces one face and portions of the four abutting faces (taking a slab shape) for $0.25 \lesssim V_M \lesssim 0.7$, forms the inverse to the rod-in-edge configuration for $0.7 \lesssim V_M \lesssim 0.9$, and forms the inverse to the cube-in-corner configuration for $0.9 \lesssim V_M$. It is speculated that results from the study for other contact angles can be used to predict the melt trajectory of a cube particle for different degrees of wetting.

3.3. Case 2: The cuboctahedron, $\Upsilon = 0.866$

The cuboctahedron is interesting because the eight {111} facets are equilateral triangles, the six {100} facets are squares, and all corners join four facets. The only other shape (in the family of $\mathcal{W}$ studied here) that shares the latter trait is the octahedron, which joins four *identical* facets. For the cuboctahedron, the majority of the total interfacial area and total interfacial free energy comes from the {100} facets.

Fig. 1 shows that six configurations comprise the cuboctahedron's equilibrium trajectory. The melt sits in one corner for the lowest melt volume fractions ($V_M < 0.06$, **I**), replaces one {111} facet and portions of the six abutting facets for $0.06 < V_M < 0.26$ (**II**), replaces one {100} facet and portions of the eight abutting facets for $0.26 < V_M < 0.42$ (**III**), forms the inverse to configuration **III** for $0.42 < V_M < 0.62$ (**IV**), forms the inverse to

II for $0.62 < V_M < 0.97$ (**V**), and forms the inverse to **I** for $0.97 < V_M$.

Like the cube, the equilibrium trajectory contains configurations for which the melt sits in one corner and its inverse. A corner configuration minimizes interfacial free energy because, as melt volume is added to **I**, melt can replace a large amount of solid interface for a relatively small increase in internal melt interface. Although increments to the melt volume in configuration **I** and its inverse give relatively small additions to the internal melt interface, these configurations appear on the equilibrium melt trajectory for smaller ranges of V_M because the cuboctahedron trajectory has lower energy configurations that are not possible in the cube.

The equilibrium trajectory of the cuboctahedron contains a configuration that produces an unexpected sequence: configuration **IV** touches all but one {100} and four {111} facets. Although the **III–IV–V** path minimizes interfacial free energy on increasing V_M, it does not follow from common logic because it requires the melt to retract from replaced interface. Such unexpected results have been noted previously [8].

3.4. Cases 3–4: The truncated octahedra, $\Upsilon = 1$ and 1.155

The equilibrium melt trajectory for the truncated octahedra resembles that of the cuboctahedron. Fig. 1 illustrates that the disparities are primarily due to particle shape. There is a fundamental difference between cuboctahedron melt configurations and truncated octahedron ones: while {100} facets of the cuboctahedron meet at a corner, those of the truncated octahedra are separated by a pair of {111} facets. Hence, for the truncated octahedra, configuration **I** puts the melt in a corner joining three, rather than four, facets. There are intermediate V_M configurations that display greater similarity to those of the cuboctahedron: configuration **II** replaces portions two {100} and two {111} facets, and configuration **III** replaces one{111} interface and portions of the six abutting facets. (Configurations **V**, **VI**, and **VII** are the inverses to configurations **III**, **II**, and **I**, respectively.)

Results for the truncated octahedra demonstrate that melt configurations preferred by the ratio of facet free energies, Υ, can differ from those preferred by the particle $\mathcal{W}$ that follows from Υ . Consider the $\mathcal{W}$ for which $1 < \Upsilon < 1.732$. The drive to selectively replace {100} interface *diminishes* as $\Upsilon \rightarrow 1.732$. This occurs because, although the interfacial free energy density of {100} interface is greater, the relative contribution of {111} interface to the total interfacial area and energy is larger, and it increases with Υ . The drive to replace {100} is also reduced by the smaller areas of and larger distances between {100} facets—melts of small V_M attempting to replace multiple {100} facets become increasingly susceptible to necking instabilities. Consequently, replacing as much solid particle/solid matrix interface as possible becomes more important than maximizing the amount of the higher-energy {100} interface replaced. The calculations support this result, showing, e.g., configurations **II**, **IV**, and **VI** to form a smaller portion of the melt trajectory for $\Upsilon = 1.155$.

3.5. Case 5: The octahedron

The octahedron is bounded by eight {111} facets, meaning that the melt can replace only one type of interface and, as for the cube, melting behavior is the product of nothing more than the particle's shape and the contact angle that the melt makes with the replaced facets. The trajectory of configurations shown in Fig. 1 indicate that, for the octahedron, the melt sits in a single corner for $V_M < 0.17$ (**I**), replaces a full {111} and portions of the six abutting facets for $0.17 < V_M < 0.83$ (**II**), and takes the inverse of **I** for $0.83 < V_M$ (**III**). Results for the octahedron display a number of interesting features, three of which are discussed below.

First, there is a configuration that appears to produce (within numerical error) the same interfacial free energy as configurations **I** and **II** at $V_M = 0.17$ but does not appear anyplace else on the equilibrium trajectory. This configuration puts the melt into two adjacent corners, so that it replaces portions of six facets. For $V_M < 0.17$, the configuration requires slightly more energy than **I**, and for $V_M > 0.17$, it requires slightly more than **II**. Because the three configurations appear to be energetically equivalent at $V_M = 0.17$ and differences in energy between them are relatively small at nearby V_M, the probability of observing the two-corner configuration (i.e., the melt in a metastable state) is relatively large for V_M near 0.17.

Second, the energy of configuration **II** decreases approximately linearly with V_M. This result is interesting because configuration **II** appears to mimic, energetically, the behavior of the cube's configuration **III** (Fig. 1). As for the cube, growth of the melt in the octahedron's configuration **II** increases the amount of solid particle/solid matrix replaced at a constant rate. However, the shape of the internal melt interface does not remain constant—it changes slightly as the melt grows due to modifications in the shape of the boundary to which it is attached (i.e., unlike the cube, when moving along the vector $\vec{v}$ pointing from the center of one face to the octahedron's center of gravity, the cross section of the octahedron in a plane perpendicular to $\vec{v}$ changes.)

Third, the transition from configuration **II** to configuration **III** requires a jump in energy. That is, the energy curve describing configuration **II** does not cross that of **III** at $V_M = 0.83$ but terminates at that V_M because configuration **II** reaches a touching instability. This jump implies that it would be necessary to increase the driving force for melting through, for instance, additional increments in temperature, because extra energy must be supplied to reach the next configuration in the melt trajectory. Al-

ternatively, the change in melting temperature with melt volume fraction should increase at this V_M.

4. Conclusions

We have demonstrated that the melting behavior of small particles embedded in the solid state depends on both particle shape and the free energy densities of the interfaces that are present during melting. The equilibrium melt trajectories for the five shapes considered result from the interplay between shape geometry and the relationship between the energy densities of five distinct interfaces.

Because the particle shapes follow from Υ through the Wulff construction, the distance between facets is dependent on their energy. Thus, for shapes containing both {100} and {111} interface, the driving force to replace the largest energy facets decreases as the relative energy densities of those facets increases, as the contribution of those facets to the total interfacial free energy diminishes and a melt that preferentially replaces them necessitate a significant amount of internal melt interface. Such a melt is typically either unstable or metastable to other configurations.

Acknowledgments

Ellen J. Siem would like to thank Samuel M. Allen and W. Craig Carter for useful discussions. This work was supported by Danish Natural Sciences Research Council. We are grateful to P. Ochin and his group (CNRS-CECM) for preparing the rapidly solidified materials and to U. Dahmen for access to the microscope (LBNL-NCEM).

References

1. W. THOMSON, *Philos. Mag. (IV)* **42** (1871) 448.
2. J. TYNDALL, *Proc. R. Soc. Lond.* **9** (1858) 76.
3. G. WULFF, *Z. Krist. Mineral* **34** (1901) 449.
4. E. JOHNSON, H. H. ANDERSEN and U. DAHMEN, Nanoscale lead and noble gas inclusions in aluminum—structures and properties, to appear in *Microscopy Research and Technique*.
5. H. SAKA, Y. NISHIKAWA and T. IMURA, *Philos. Mag. A* **7**(6) (1988) 895.
6. K. SASAKI and H. SAKA, *Philos. Mag. A* **63**(6) (1991) 1207.
7. K. SASAKI and H. SAKA, *Microsc. Microanal. Microstruct.* **4** (1993) 287.
8. E. J. SIEM and E. JOHNSON, Melting of embedded anisotropic particles: PbIn inclusions in Al, to appear in *Philos. Mag.*
9. E. JOHNSON, A. JOHANSEN, U. DAHMEN, S. CHEN and T. FUJII, *Mater. Sci. Eng. A—Struct.* **304–306** (2001) 187.
10. H. GABRISCH, L. KJELDGAARD, E. JOHNSON and U. DAHMEN, *Acta Mater.* **49** (2001) 4259.
11. L. E. MURR, *Interfacial Phenomena in Metals and Alloys* (Herndon, Virgina: Techbooks, 1975).
12. A. R. ROOSEN, R. P. MCCORMICK and W. C. CARTER, *J. Comp. Mat. Sci.* **11**(1) (1998) 16. http://www.ctcms.nist.gov/wulffman/ Source code and manual freely available.
13. K. A. BRAKKE, The surface evolver, *Exp. Math.* **1**(2) (1992) 141. http://www.susqu.edu/facstaff/b/brakke/evolver/ Source code and manual freely available.
14. D. CHATAIN, P. WYNBLATT, S. HAGÈGE, *et al.*, *Interf. Sci.* 9(3–4) (2001) 191.